NASA TECHNICAL NOTE

NASA TN D-1978

NASA TN D-1978

THERMAL RADIATION FROM ABLATION PRODUCTS INJECTED INTO A HYPERSONIC SHOCK LAYER

by Roger A. Craig and William C. Davey;
Ames Research Center,
Moffett Field, California

NATIONAL AERONAUTICS AND SPACE ADMINISTRATION • WASHINGTON, D. C. • SEPTEMBER 1963

TECHNICAL NOTE D-1978

THERMAL RADIATION FROM ABLATION PRODUCTS INJECTED INTO A HYPERSONIC SHOCK LAYER

By Roger A. Craig and William C. Davey

Ames Research Center
Moffett Field, California

NATIONAL AERONAUTICS AND SPACE ADMINISTRATION

NATIONAL AERONAUTICS AND SPACE ADMINISTRATION

TECHNICAL NOTE D-1978

THERMAL RADIATION FROM ABLATION PRODUCTS INJECTED INTO A HYPERSONIC SHOCK LAYER

By Roger A. Craig and William C. Davy

SUMMARY

A study was made of the thermal radiation associated with the ablation of plastic materials. As ablation product materials diffuse into the boundary layer, they become possible important sources of radiant energy. This radiation may be due to either the increase in temperature of the ablation products or to chemical reactions occurring in the boundary layer.

For the tests, small blunt-nosed projectiles were launched at high velocities past photoelectric devices which recorded the resulting radiation. A simple mathematical model was developed to describe the boundary injection-diffusion process, and equations were derived for the surface heating from this source for vehicles of spherical geometry. The test results were used to evaluate empirical constants in the equations.

Three ablation materials were tested: lexan, a polycarbonate resin; General Electric Company Century Series 124, a char-forming plastic; and a high-density polyethylene.

Predictions of the stagnation-point heating of large-sized vehicles based on the above tests and mathematical model indicate that the radiative heating of ablation products varies over a wide range depending upon the ablation material. For at least one material the radiant heating is of the same magnitude as the convective heating.

INTRODUCTION

Because of the current interest in thermal radiation effects during hypersonic flight, an investigation of the thermal radiation from ablation products in the stagnation region of blunt bodies is being conducted in ballistic ranges at the Ames Research Center. The present paper is a preliminary report of results obtained to date for three ablation materials in the velocity range of 4.5 to 7.5 km/sec. The test technique consists of launching small diameter plastic or metal models at high velocities and measuring the resultant radiation with photoelectric devices. Previous publications describing this work are references 1, 2, and 3. References 1 and 2 describe air radiation from the shock layer and

reference 3 describes radiation from the wake. During the progress of these tests, it was noted that the spectra observed for a given test condition were a function of the model material, and, because of the ablation occurring on the front face of the model, these anomalies were attributed to foreign material radiating in the boundary layer. In certain instances, the intensity of the radiation presumed to be due to the foreign material was equal to or greater than that due to air. The question was raised as to the importance of the ablation product radiation to the total surface heating for full-scale vehicles. A study was therefore undertaken to quantitatively evaluate ablation product radiation as a source of radiative heating to vehicles in hypersonic flight.

Prior work, both analytical and experimental, related to the radiation associated with the ablation process is described in references 4 and 5. The experiments consist of measurements of the radiation resulting from the ablation of plastic samples in a supersonic air stream heated by an arc discharge. The enthalpy range of the tests was equivalent to velocities from 1.5 to 5 km/sec. In the analysis of these data, the radiation was assumed to come from the solid surface of the material under test.

The present investigation included both experimental work to measure the radiation from the ablation products at model scale and theoretical work to estimate the radiation from this source at full scale. The experiments were made with three ablating plastics and with aluminum (which did not ablate under the test conditions) at velocities from 4.5 to 7.6 km/sec and at free-stream air densities from 0.02 to 0.2 amagat.

SYMBOLS

C	boundary-layer-edge velocity gradient, sec^{-1}
E	radiant output per unit mass, watts/gm
k	ratio of universal gas constant to molecular weight
K	radiation constant, watts $(cm)^{3\zeta}(gm)^{-(\zeta+1)}(^{o}K)^{-\xi}$
$\dot{m}$	mass injection rate per unit surface area, gm/cm^2-sec
M.W.	molecular weight
p	pressure, gm/cm^2
Pr	Prandtl number
$\dot{q}$	surface heating rate, $watts/cm^2$
r	radius from line of symmetry to the location s on the surface of vehicle, cm
R	body nose radius of vehicle, m

s	distance along body surface, measured from stagnation point, cm
Sc	Schmidt number
T	temperature, ^{o}K
u	velocity in s direction, km/sec
V	velocity, km/sec
W	mass fraction of ablation products in the boundary layer
y	distance measured normal to surface, cm
Y	value of y where $W = 0$, cm
z	transformed normal distance, $\rho_w \, dz = \rho \, dy$
δ	boundary-layer thickness
ΔT	temperature difference across boundary layer, $T_e - T_w$, ^{o}K
λ_o	wavelength of peak response of the photodetector, microns
Φ	universal gas constant
ζ	exponential dependence of E on density
ξ	exponential dependence of E on temperature
ρ	density, gm/cm^3
σ	angle subtended by radius from axis to location s on surface
$( )^*$	value at the corner of the face (taken to be the sonic point)

Subscripts

a	ablation
c	convection
e	edge of boundary layer
T	temperature
w	wall
W	ablation product mass fraction
∞	free stream

1 ablation products

2 air

o standard atmospheric conditions

TESTS AND APPARATUS

Small models were launched from a light-gas gun through air at selected pressures and the radiation from the model flow field was measured by photometric devices in the test section. The model launcher used is a two-stage, shock-heated, light-gas gun with a bore diameter of approximately 7 mm (refs. 1, 2, 3). The test section is located 6 meters beyond the muzzle and is isolated from the muzzle blast by means of a blast deflector plate and a vented section.

The main instrumentation (fig. 1) consisted of the spectral detectors for measuring radiation. In addition, two shadowgraph stations were equipped with electronic timing devices (for velocity and attitude measurements) and a Kerr cell shutter camera (for single frame photographs of luminous material near the model). The spectral detectors used in these experiments, one of which is shown schematically in figure 2, were multiplier phototubes in combination with narrow pass optical filters. The response of each combination was therefore limited to a narrow spectral range. By the use of eight such units, low resolution spectra of the radiation generated by the models were obtained. Shown in the table below are the characteristics of the phototube-filter combinations. The band passes listed are the widths between the half-maximum sensitivity points.

Maximum sensitivity, wavelength	Band pass	Tube type		Photoemissive surface
0.235μ	0.049μ	RCA	1P28	S-5
.265μ	.049μ	RCA	1P28	S-5
.312μ	.056μ	RCA	1P28	S-5
.369μ	.038μ	Dumont	6467	S-11
.460μ	.026μ	Dumont	6467	S-11
.518μ	.059μ	Dumont	6467	S-11
.661μ	.077μ	Dumont	K1430	S-1
.942μ	.175μ	Dumont	K1430	S-1

The slits, shown in figure 2, limit the field of view of the phototube to approximately 1 cm of flight path. The geometry of the slits permits the entire shock layer to be viewed, and the shock-layer and wake radiation to be distinguished.

Because the sensitivity of a multiplier phototube is strongly dependent on the high voltage supplied to the dynodes, the power supplies were carefully regulated and monitored. During many of the tests, neutral optical filters were used to avoid saturation and resulting nonlinear operation of the phototubes. All filters and phototubes were carefully calibrated by procedures described in appendix A.

Models of two different geometries were used, as shown in figure 3. In order to investigate the relationships between model material and ablation-product radiation, four materials were tested: aluminum, the polycarbonate lexan, polyethylene, and the General Electric Company Century Series plastic 124 (hereinafter referred to as G.E. 124). Some materials which would not withstand launching stresses in the basic configuration were launched successfully when supported by a sabot. The sabots were made of lexan. For all the data in this report, the sabots were separated sufficiently from the model at the measuring station so that the model radiation could be monitored without interference from the sabot.

The composition of the test air was monitored and no appreciable contaminants were found.

TEST RESULTS

During the tests, the responses of the phototubes were displayed on oscilloscopes. These displays were photographically recorded and a complete set from a typical test is shown in figure 4. The wavelength of maximum sensitivity of each spectral detector is noted below each record. At wavelengths in the ultraviolet, the signal obtained consists of a single pulse which is interpreted as resulting from energy radiated from the shock layer. At the longer wavelengths, the signal undergoes a distinct change in wave form; this change includes the development of a small rise immediately added to the initial pulse and the appearance of a second pulse due to energy radiated from the wake. The first rise of the initial pulse is from the nose region traversing the region of partial view (fig. 2). The further rise of this pulse occurs as the luminosity along the sides of the model comes into view. The relationship between phototube response and model luminosity is illustrated by the self-luminous photograph and the oscilloscope record in figure 5. The time scale in the oscilloscope record has been adjusted to match the distance scale of the photograph. The photograph was taken with the Kerr cell shutter camera at 50 nanosecond exposure time with film responsive in the wavelength region from 0.42 to 0.6μ.

The basic data of the investigation which consist of measurements of the radiation from the nose region were obtained by reading the height of the first pulse and, by the method outlined in appendix A, converting to a radiant intensity of the source in watts/micron. The proper reading point for the height of the pulse is the end of the first rise, taken to be the entire nose region in full view, but before the radiation from the model sides is in full view.

Typical results obtained by this procedure are shown in figure 6 for the four materials tested at three air densities. The short horizontal bars in the figure are the data reported in watts/micron radiated into 4π steradians. The lengths of the bars are the band pass widths of the detectors as defined earlier. Lines have been faired through the data to approximate the spectra.

The expected radiation from the air in the shock layer is shown superimposed on the data for the aluminum models. The prediction is taken from reference 6 for air at equilibrium. The predicted level of radiation for air agrees well with the total shock-layer-radiation data for the aluminum models at the two higher air densities. The disagreement at the lowest density is attributed to

nonequilibrium air radiation (ref. 2). Some disagreement is noted, at all densities, however, at wavelengths greater than 0.5μ. Whether this difference indicates a deficiency of the air-radiation prediction is not known at this time. Calculations made for the surface temperatures of the aluminum models indicated that melting temperature was never reached when the models passed the radiation detectors. Therefore, it is concluded that no aluminum ablation products were present and the spectra are representative of air.

Based on the above, the spectra obtained with the aluminum models were subtracted from those obtained with the plastic models to remove the air-radiation contribution. (A slight adjustment was necessary to correct for the small difference in size between the aluminum models with sabots and the full-bore plastic models.) The results of this procedure are shown in figure 7.[1] It is clear from this figure that a considerable quantity of radiation in excess of that expected from the air is observed with these materials, and the amount is strongly dependent on the material itself.

The non-air radiation can be due to either the hot ablating surface or to the products of ablation in the boundary layer. If it is due to the former, then it is a cooling mechanism for the heat shield. If the latter is correct, then it constitutes a potential mechanism for additional heat input to the body.

A simple test was devised to determine the origin of the non-air radiation. It consisted of launching models with effectively no projected nose area (i.e., right circular cylinders) and contrasting the measured radiation with that measured from spherical faced models. If the non-air radiation were predominantly coming from the hot surface, the observed output would be severely attenuated because the projected area of the model surface viewed by the detectors would be essentially zero. Figure 8 gives results of these tests with lexan models together with results from one lexan model with the usual geometry chosen for similar test conditions. Flattening the model face increased the radiation observed in spite of the facts that less surface area was in view of the radiation detectors and the convective heating rate was lower. In addition, an effort was made to possibly attribute this radiation in part to a radiating surface in view of the detectors such as the corners which could ablate more rapidly than the stagnation area because of high convective heating. For the 6.72 km/sec test it was estimated that the corner rounded to give a projected area of not more than 10^{-3} cm^2 during the flight time. Assuming a surface temperature equal to melting carbon, and an emissivity of 1.0, a surface of this size could radiate only 5 percent of the observed amount. This shows that the non-air radiation emanated primarily from ablation products which are injected into the boundary layer. The same tests were conducted on G.E. 124 and polyethylene with analogous results.

---

[1]Because of the small variation in velocity between various tests, a small velocity correction was made before subtracting the air radiation from the total spectrum obtained from the plastic materials. Reference 1 shows that over the range of these tests the air radiation is proportional to the eighth power of the velocity. This relationship was therefore used for the velocity correction. Generally, these corrections were less than 15 percent, but in a few instances were as high as 60 percent.

Another basic question was whether or not steady-state ablation was established for the plastic models in these tests. For the case of noncharring materials, the surface temperatures of the models were calculated as a function of flight-path distance for the test conditions of lowest heating rates. It was found that the model always traveled at least 20 times the distance required for the surface temperatures to reach that necessary for ablation, intimating that sufficient time is available to establish steady-state ablation.

To calculate the quasi-steady-state conditions of the char-forming G.E. 124, a model was hypothesized as follows: Because of the very short time of flight (1 millisecond) the char-spallation sequence was assumed to be in its initial cycle (ref. 7). The char thickness was assumed to increase linearly along the flight path as the plastic pyrolized, and the preheat time was assumed short compared to the flight time. Char thicknesses were calculated and were typically of the order of 10^{-3} cm at the test section. Because the char was very thin, it was taken to have little effect on the ablation properties of the material, influencing only wall temperatures.

The data of figure 7 were converted to average heating rates of the model face by integrating the spectra from 0.45μ to 1.1μ and dividing half the integral by the surface area that the observed radiation falls on, namely, the curved surface of the model face. Because of the data scatter, intensity measurements were limited to spectral regions where the ablation product radiation was at least greater than the uncertainty of the measurements of the air radiation; hence, the lower limit of integration is 0.45 micron. It is to be noted, however, that in some specific tests ablation product radiation below this limit appears to be measured. It is concluded that this additional apparent radiation is due to scatter in the data, and is not interpreted as ablation product radiation. The upper limit represents the long wavelength cut-off of the instrumentation. Because of this restricted wavelength region, the resulting heating rates represent lower limits of the actual ablation product radiation heating rates. Allowance was made for that portion of the radiation hidden from the detector by the convex model face. Results of the integration are given in table I along with other parameters of interest for each test. It is apparent that under the test conditions, the amount of radiation from lexan ablation products was considerably more than radiation from ablation products of the other two materials.

ANALYSIS

It is not possible at the present state of knowledge to treat in complete detail the physical processes involved in ablation product radiation which would require taking into account specific chemical reactions, species present, etc. Instead, in the analysis which follows, consideration is given to gross boundary-layer processes which affect this radiation. The analysis relies on the present experiments and has as its objective the rational extrapolation of these experimental results to other air densities and larger vehicles.

Mathematical Model

As was demonstrated in the last section, the non-air radiation measured during the present study could not have originated from the model surface; hence, the following analysis is based on the initial assumption that the radiant sources are ablated materials which are diffusing into the boundary layer over the model face. It is further assumed for simplicity that all important chemical reactions occur near the wall; subsequent reactions do not seriously alter the radiant power output.

In general, one would expect the total power output per unit mass of foreign material (defined as unreacted ablation products and ablation products which have reacted with air) in the boundary layer to take the form $E' = K'\varphi(T)$ where $\varphi(T)$ is some pure function of the temperature. It is more convenient, however, to correlate the radiation on the basis of the mass loss from the model surface instead of the mass of foreign products in the boundary layer since it is very difficult to predict the extent of chemical reactions at the wall and, hence, the actual mass of foreign materials present in the boundary layer. However, these reactions may be sensitive to changes in density; therefore any correlation based on mass loss must provide for a density dependence.

The following expression is then postulated as the power output per unit mass of ablation products (ablation product being defined as the material in the boundary layer which was originally part of the surface):

$$E = K\rho^{\zeta}T^{\xi} \tag{1}$$

where the effect of any chemical changes will appear especially in the magnitude of ζ. Note that if ζ is zero, the density term in the above equation is removed and this infers that there are no chemical reactions present, or, if there are, they produce no change in the radiant energy output, or the reactions are not density dependent. Chemical reactions may also contribute to the magnitude of ξ; however, no particular interpretation may be assigned to any specific value of ξ.

The local heating, $\dot{q}_a$, due to radiation from a boundary layer, which is thin compared to its lateral dimensions, is obtained by taking half of the integral of the radiant output as a function of normal distance to the wall, namely,

$$\dot{q}_a = \frac{1}{2}\int_0^Y WE\rho \, dy \tag{2}$$

where W is the mass fraction of ablation products in the boundary-layer mixture, ρ is the total gas density (air and ablation products), both being functions of y, and Y is the value of y when $W = 0$.

We introduce a transformed distance z which is defined by the equation

$$\rho_w \, dz = \rho \, dy \tag{3}$$

where ρ_w is the value of ρ at $y = 0$.

We now assume a linear dependence of W and T on this transformed variable:

$$\frac{T_e - T}{T_e - T_w} = 1 - \frac{z}{\delta_T} \tag{4}$$

$$\frac{W}{W_w} = 1 - \frac{z}{\delta_W} \tag{5}$$

As used here, the temperature boundary-layer thickness, δ_T, is defined as that value of z where $T/T_e = 0.99$ and similarly the concentration boundary-layer thickness, δ_W, is that value of z where $W/W_w = 0.01$.

These assumptions appear to be reasonable in the light of results obtained by Howe (ref. 8) and Roberts (ref. 9). Using a detailed method to calculate the mass distribution of foreign species injected into the boundary layer, Howe found a nearly linear distribution of W with respect to η, which is a transformed distance related to z by a constant determined by vehicle geometry. Roberts, using the same linear assumptions as above, developed equations which describe the heat-transfer characteristics of a boundary layer with mass injection. He found that these equations gave results that agreed very well with boundary-layer heat transfer calculated by several exact methods.

If one assumes the mixture to be a perfect gas, in order to use simple relationships between the state variables, the equation of state can be written

$$p = (k_1\rho_1 + k_2\rho_2)T$$

Here k_1 is the gas constant divided by the average molecular weight for the ablation products and ρ_1 is the partial density of the ablation products. The terms k_2 and ρ_2 have analogous meanings for air.

Since $\rho_1 = W\rho$ and $\rho_2 = (1 - W)\rho$, the equation of state can be written in the form

$$p = (k_3W + k_2)\rho T$$

where

$$k_3 = k_1 - k_2$$

Thus the total density may be written as a function of the concentration as

$$\rho = \frac{p}{(k_3 W + k_2)T} \tag{6}$$

By substituting equations (1), (3), (4), (5), and (6) into (2) and retaining W as the variable of integration, we get

$$\dot{q}_a = \frac{K\rho_w \delta_W p^{\zeta}}{2W_w} \int_0^{W_w} \frac{\left[T_e + \Delta T \left(\frac{\delta_W}{\delta_T} - 1 - \frac{W}{W_w}\frac{\delta_W}{\delta_T}\right)\right]^{\xi-\zeta}}{(k_2 + k_3 W)^{\zeta}} W \, dW \tag{7}$$

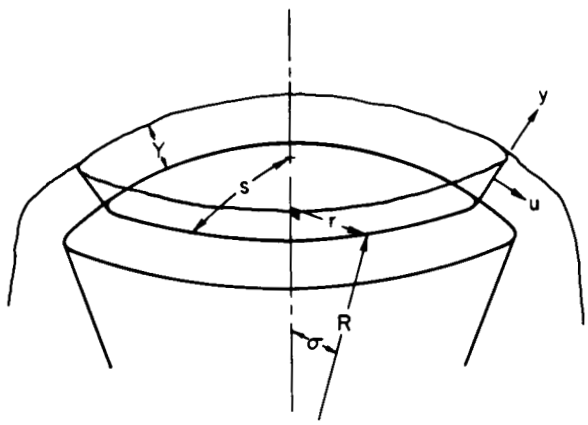

At this point we introduce the concept of a mass balance to determine an expression for δ_W in terms of ratios of boundary-layer thicknesses. The sketch of the forward surface of a vehicle with spherical geometry will be helpful in visualizing the following development.

The mass injected into the boundary layer from $s = 0$ to $s = s$ (s is the distance along the body surface measured from the stagnation point) is the integral over the surface $\int_0^s \dot{m}\, da$, where $\dot{m}$ is the mass injection rate per unit surface area. The ablation material convected through a surface normal to the body at $s = s$ is $2\pi r \int_0^Y Wu\rho \, dy$ evaluated at s. Here r is the radius from the line of symmetry to the plane s, and u is the gas velocity parallel to the surface. Noting that $r = R \sin\sigma$ and recalling that $\rho\, dy = \rho_w\, dz$ we may equate the two above expressions

$$\int_{\substack{0 \\ \text{surface}}}^{s} \dot{m}\, da = \left(2\pi R \sin\sigma\, \rho_w \int_0^{\delta_W} Wu\, dz\right)_{\text{at } s}$$

Using equation (5), we write

$$\int_{\substack{0 \\ \text{surface}}}^{s} \dot{m}\, da = \left[2\pi R \sin\sigma\, \rho_w W_w \int_0^{\delta_W} \left(1 - \frac{z}{\delta_W}\right) u\, dz\right]_{\text{at } s} \tag{8}$$

As before, we linearize u on z; $u/u_e = z/\delta_u$. Here δ_u is defined as that value of z when $u/u_e = 0.99$. Equation (8) may be integrated and written as

$$\int_{\substack{0 \\ \text{surface}}}^{s} \dot{m}\, da = \left[\frac{1}{3}\pi R \sin\sigma\, \rho_w W_w u_e \left(\frac{\delta_W}{\delta_u}\right) \delta_W\right]_{\text{at } s} \tag{9}$$

If the analysis is restricted to relatively blunt configurations, the convective heat transfer is not expected to vary more than 30 percent from that at the stagnation point (ref. 10). To within this accuracy then, the mass injection rate may be considered a constant over the surface. The left side of equation (9) may then be approximated by

$$\int_{\substack{0 \\ \text{surface}}}^{s} \dot{m}\, da = [2\pi R^2(1 - \cos\sigma)\dot{m}]_{\text{at } s} \tag{10}$$

We note also that, for blunt configurations, the boundary-layer edge velocity, u_e, is a nearly linear function of s (ref. 11), increasing from 0 at the stagnation point to sonic velocity at the corner. The edge velocity may then be written

$$u_e = Cs = CR\sigma \tag{11}$$

where C is the velocity gradient. Thus, by utilizing equations (9), (10), and (11) we can write the continuity equation:

$$\dot{m}\left(\frac{1 - \cos\sigma}{\sigma \sin\sigma}\right) = \frac{1}{6}\rho_w W_w C \left(\frac{\delta_W}{\delta_u}\right)\delta_W$$

The trigonometric portion of the above expression is a slowly changing function of σ, having a value of 0.500 at $\sigma = 0$, and a value of 0.527 at $\sigma = 45^\circ$; it therefore may be replaced by 1/2 without introducing significant error. The continuity equation then becomes

$$\delta_W = \frac{3\dot{m}}{\rho_w W_w C}\left(\frac{\delta_u}{\delta_W}\right) \tag{12}$$

This expression for δ_W may then be used in equation (7) to obtain the heating equation in complete form:

$$\dot{q}_a = \frac{3}{2}\frac{Kp^{\zeta}\dot{m}}{W_w{}^2 C}\left(\frac{\delta_u}{\delta_W}\right)\int_0^{W_w} \frac{\left\{T_e + \Delta T\left[\left(\frac{\delta_W}{\delta_T}\right) - 1 - \frac{W}{W_w}\left(\frac{\delta_W}{\delta_T}\right)\right]\right\}^{\xi-\zeta}}{(k_2 + k_3 W)^{\zeta}} W\, dW$$

This equation can be rewritten

$$\dot{q}_a = \frac{3}{2}\frac{Kp^{\zeta}\dot{m}}{C}\left(\frac{\delta_u}{\delta_W}\right)\frac{1}{W_w^2}\int_o^{W_w}\frac{\left\{T_e + \Delta T\left[\left(\frac{\delta_W}{\delta_u}\right)\left(\frac{\delta_u}{\delta_T}\right) - 1 - \frac{W}{W_w}\left(\frac{\delta_W}{\delta_u}\right)\left(\frac{\delta_u}{\delta_T}\right)\right]\right\}^{\xi-\zeta}}{(k_2 + k_3 W)^{\zeta}} W\,dW \tag{13}$$

In reference 9, Roberts has shown that the ratio of the concentration boundary-layer thickness to the velocity boundary-layer thickness is $\delta_W/\delta_u = (Sc_w)^{-0.3}$ and since the Schmidt number for the mixture at the wall is estimated to lie between 0.8 and 2, it will be assumed, for the sake of simplicity, that $\delta_W = \delta_u$. The ratio of the velocity boundary-layer thickness to the temperature boundary-layer thickness is also nearly 1 since, again, in reference 9, $\delta_u/\delta_T = (Pr_w)^{0.3}$ and the Prandtl number is estimated to lie close to 1. With these two relationships we can write equation (13) as

$$\dot{q}_a = \frac{3}{2}\frac{K\dot{m}p^{\zeta}}{C}\frac{1}{W_w^2}\int_o^{W_w}\frac{\left(T_e - \frac{\Delta T}{W_w}W\right)^{\xi-\zeta}}{(k_2 + k_3 W)^{\zeta}} W\,dW \tag{14}$$

Recalling that k_3 is defined by $k_3 = k_1 - k_2$, and k_1 and k_2 are ratios of the universal gas constant to the molecular weights, we can write the denominator in the integral as

$$\Phi^{\zeta}\left[\frac{1}{(M.W.)_2} + \left(\frac{1}{(M.W.)_1} - \frac{1}{(M.W.)_2}\right)W\right]^{\zeta}$$

A value of 29 is appropriate for $(M.W.)_2$ and from reference 12, 36 seems to be a representative value[2] of $(M.W.)_1$. These values make it apparent that k_3W is small compared to k_2. In fact, if the denominator is set equal to k_2^{ζ} and if $T_w^{\xi+1}$ is very small compared to $T_e^{\xi+1}$ the heating equation may be integrated in closed form to obtain

$$\dot{q}_a = \frac{3}{2}\frac{K\dot{m}}{C}\rho_e^{\zeta}\frac{T_e^{\xi+2}}{(\Delta T)^2(\xi - \zeta + 1)(\xi - \zeta + 2)} \tag{15}$$

To ascertain the error introduced by this simplification, equation (14) was machine-programmed and evaluated for the above-stated values of k_1 and k_2.

---

[2]In reference 5, the charring ablation process was simulated experimentally and under certain conditions a value of approximately 5 was obtained for the molecular weight of the ablation products. This value used in evaluating $\dot{q}_a$ from equation (14) resulted in predicted heating rates only 8 percent lower than those obtained using a molecular weight of 36.

When typical values for the other parameters were used, the value of $\dot{q}_a$ given by equation (15) was found to be within 5 percent of the value of $\dot{q}_a$ given by equation (14).

The effects of changes in vehicle size on $\dot{q}_a$ are directly apparent from equation (15) because only $\dot{m}$ and C are sensitive to vehicle size. If the mass injection rate, $\dot{m}$, is controlled primarily by convective heating, $\dot{m}$ is proportional to $R^{-1/2}$ and, if the sonic point is fixed somewhere near the corner of the face, 1/C is proportional to R so that equation (15) reduces to $\dot{q}_a$ proportional to $R^{1/2}$.

Application to Test Data

In order to use the test data to evaluate the empirical constants, equation (15) is written in logarithmic form. Since the data cover a relatively small temperature range, ξ cannot be deduced directly without large uncertainty. Hence, an appropriate value will be assumed and the following equation solved for ζ and K:

$$\log\left[\frac{2\dot{q}_a C(\Delta T)^2}{3\dot{m}T_e^{\xi+2}}\right] = \log K + \zeta \log \rho_e - \log(\xi - \zeta + 1) - \log(\xi - \zeta + 2)$$

Further, if the first two terms of the rapidly convergent series expansion for $\log(a + x)$ are used to expand the last two terms in the above equation, and if ζ is anticipated to be much smaller than $2(\xi + 1)$, the above equation is written as

$$\log\left[\frac{2\dot{q}_a C(\Delta T)^2(\xi + 1)(\xi + 2)}{3\dot{m}T_e^{\xi+2}}\right] = \log K + \zeta\left[\log \rho_e + 0.434\left(\frac{1}{\xi + 1} + \frac{1}{\xi + 2}\right)\right] \quad (16)$$

Thus, it is apparent from the above equation that if X_1 is represented as a function of X_2, where

$$X_1 = \log\left[\frac{2C\dot{q}_a(\Delta T)^2(\xi + 1)(\xi + 2)}{3\dot{m}T_e^{\xi+2}}\right]$$

and

$$X_2 = \log \rho_e + 0.434\left(\frac{1}{\xi + 1} + \frac{1}{\xi + 2}\right)$$

the resulting function is in slope-intercept form, where ζ is the slope and $\log K$ is the intercept.

At this point it is appropriate to discuss briefly the methods used for calculating the values of the parameters appearing in X_1 and X_2. Parameters not dependent upon the material but, rather, on the state of the air in the shock layer are the temperature and density at the edge of the boundary layer, T_e and ρ_e, and the velocity gradient along the surface at the edge of the boundary layer, C. The first two of these values, T_e and ρ_e, are taken to be those behind a normal shock wave for high temperature air (ref. 13). The velocity gradient, C, was calculated assuming a linear velocity history along the edge of the boundary layer from the stagnation point to the sonic line.

The mass injection rate, $\dot{m}$, and the temperature difference across the boundary layer, ΔT, are dependent upon the properties of the ablating material. Reference 14 was used to calculate $\dot{m}$ for polyethylene and lexan tests; information was not available for calculating $\dot{m}$ for G.E. 124, so it was assumed to be like lexan in this respect. To calculate the temperature difference across the boundary layer, a knowledge of the surface temperature of the ablating material is required. Reference 15 presents the surface temperature of ablating polyethylene. The surface temperature of lexan was unknown but it was assumed that lexan would behave similarly to polyethylene. It should be pointed out that the temperature difference across the boundary layer will be of the order of 6000° K so that an error of 200° K in estimating the surface temperature will change the temperature difference by only 3 percent. The method used in reference 7 for calculating surface temperature of charring ablators was employed to calculate the surface temperature of G.E. 124.

Before values of X_1 and X_2 can be calculated and plotted, ξ, the remaining empirical constant, must be determined. The range of test velocities and consequent variation in T_e was not considered large enough to evaluate ξ with precision. Reference 16 presents theoretical and empirical bases for assigning a value of 4 to this parameter. Since an uncertainty in ξ will not critically affect extrapolations of ablation product radiation heating rates as long as predictions are not made to velocities greatly different from those of the tests, a value of 4 was chosen. (In the evaluation of ξ from the lexan data the values of K and ζ, shown below, gave 3.5 ± 1.)

Each parameter required for evaluating X_1 and X_2 in equation (16) was calculated for the tests and is listed in table I. Test values of X_1 and X_2 are shown in figure 9. The empirical constants, K and ζ, are then found to be as follows

	K	ζ
Lexan	7×10^{-8} (average)	0 (average)
G.E. 124	2×10^{-8}	.12
Polyethylene	6×10^{-7}	.66

In this figure, the large symbols used for the lexan data represent an arithmetic average of the data at each of the three test densities. The actual test values are indicated by the smaller symbols. It may be seen that the possible value

of ζ for lexan could range from -0.18 to +0.22, with the value of 0 being indicated by the average points. The range of possible values of ζ for lexan indicates that the accuracy in determining ζ by the present method is approximately ±0.2. It should, therefore, be noted that ζ for G.E. 124 could also vanish; however, the determined value of ζ for polyethylene is almost certainly greater than zero. This is significant inasmuch as it indicates that the density dependence of the chemistry of ablation products is different for polyethylene than for lexan or G.E. 124 because of the chemical dissimilarity of polyethylene and the other two plastics.

Application to Large Size Vehicle

To assess the importance of ablation-product radiative heating for large size vehicles, equation (15) was evaluated for a vehicle with a 5-meter nose radius; the convective heating only was used to calculate the mass injection rate, ignoring radiative heating from air or ablation products. If these radiative sources become important, they can greatly increase the ablation rate, since there is negligible blocking of radiation by ablation products in the boundary layer.[3] The flight conditions used in these calculations were an altitude of 70 km and a velocity of 7 km/sec. The experimentally determined values of K and ζ for each of the ablation materials tested were used in these calculations. The assumption is made in the analysis that ζ is a constant over the extrapolated range, depending only on material. The actual full-scale heating may depart considerably from the derived model if, for example, radical changes in the chemistry of ablation product radiation occur in the extrapolated range. The calculated ablation product radiation is listed below together with the heating from air radiation and the cold wall convective heating. It is to be noted that for some materials the ablation product radiation can exceed the air radiation, and the resultant heating can be a substantial fraction of the cold wall convective heating. Also to be noted is the wide range of heating rates, depending on ablator material. The ablation product radiation stated for lexan under these conditions is high enough to be self-aggravating as defined in the footnote in this section, if the surface absorptivity is greater than a few tenths.

The local exponential dependence of the ablation product radiation on free-stream velocity and density was calculated and is included.

---

[3]It can be shown by writing equation (15) in difference equation form, and including the ablation product radiation to calculate the mass loss, that unless

$$\alpha(\dot{q}_a/\dot{m}) < h$$

where α is the absorptivity of the surface, h is the heat of ablation, and $(\dot{q}_a/\dot{m})$ is taken directly from equation (15), the process will be self-aggravating and the heating will approach limits imposed by available energy in the airstream.

Material or heat source	$\dot{q}$, watts/cm^2	Exponential dependence on - Velocity	Density
Lexan	24	2.6	0.67
G.E. 124	1.5	2.6	.77
Polyethylene	.043	3.0	1.3
Air radiation	.67		
C. W. convection	35		

The exponential dependence on velocity of ablation product radiation varies with velocity because of the varying relationship that exists between velocity and temperature of shock heated air. The exponential dependence on density is, as expected, strongly influenced by the value of ζ for a specific material, since the boundary-layer-edge density is nearly a linear function of the free-stream density.

CONCLUDING REMARKS

In the foregoing analysis a source of vehicle heating not ordinarily considered was investigated - the thermal radiation from the gaseous products injected into the boundary layer by the ablation process. Tests conducted on small size plastic and metal models showed that important amounts of radiation can be contributed by these products. The experimental data were used to evaluate empirical constants in a derived ablation radiative heating equation. From the resulting equation predictions for heating from this source were made for a large vehicle.

The results indicate that the ablation product radiative heating on a large vehicle can be a substantial fraction of the total heating, depending critically on the flight conditions and heat shield material; in some instances, this heating exceeds the air radiative heating.

The total heating is not necessarily the sum of all heating components presented. Each process, lowering the available energy in the shock layer, tends to moderate the other; hence, the total heating should be expected to be somewhat less than the component sum.

Since this study was a preliminary investigation of the ablation product radiative heating, and the extrapolations on size and density were made to several orders of magnitude beyond the test data, further investigations are necessary, particularly at lower densities, at higher velocities, and with larger size models. Materials representative of current ablative heat-shield material should be tested since it has been shown that the ablation product radiative heating is very strongly dependent on material.

Ames Research Center
National Aeronautics and Space Administration
Moffett Field, Calif., May 28, 1963

APPENDIX A

CALIBRATION OF SPECTRAL RADIATION DETECTORS

ABSOLUTE SPECTRAL CALIBRATION

The absolute spectral response of a detector is determined by the narrow pass optical filter, the spectral response of the photocathode, the amplification of the multiplier phototube, and the construction of the voltage divider circuit.

Relative spectral response, $R(\lambda)$, of a spectral detector was defined by the formula

$$R(\lambda) = \frac{R'(\lambda)T(\lambda)}{[R'(\lambda)T(\lambda)]_{max}}$$

where $R'(\lambda)$ is the relative spectral response of the unfiltered photocathode and $T(\lambda)$ is the spectral transmission of the narrow pass filter.

The absolute sensitivity of a detector is obtained by irradiating the detector from a unit distance with a radiant source, $W(\lambda)$, of known absolute spectral intensity. The voltage output is then

$$e = K \int_0^\infty W(\lambda)R(\lambda)d\lambda$$

where K is the absolute sensitivity of the detector to radiant energy and has units of watts/volt. Since e, $W(\lambda)$, and $R(\lambda)$ are known, we can calculate K. When recording the radiant output from an unknown source, $J'(\lambda)$, we make the following approximation

$$J(\lambda_o) \int_0^\infty R(\lambda)d\lambda \sim \int_0^\infty J'(\lambda)R(\lambda)d\lambda$$

where λ_o is the center of the interval where $R(\lambda)$ is nonzero. An average radiant flux for this interval is then represented by $J(\lambda_o)$.

The subsequent output voltage is then

$$e = K \int_0^\infty J'(\lambda)R(\lambda)d\lambda = KJ(\lambda_o) \int_0^\infty R(\lambda)d\lambda$$

and $J(\lambda_o)$ follows directly.

A more general treatment of calibration of photodetectors will be found in reference 17.

PHOTOCATHODE SATURATION

Each detector was calibrated to determine the maximum output voltage it will produce before the output becomes a nonlinear function of the incident radiation.

A short-duration, high-intensity light pulse which simulated in duration and shape the radiation measured during the tests was imaged through a lens on the photocathode. An iris in the lens varied the intensity. This configuration was then used to measure the apparent transmission of a neutral pass optical filter of 10- to 20-percent transmission. The apparent transmission is given by

$$\text{Apparent transmission} = \frac{\text{Output voltage with filter in light path}}{\text{Output voltage without filter in light path}} = \frac{V_{in}}{V_{out}}$$

When the light intensity is raised to the extent that the detector is saturated, V_{out} is no longer a linear function of the incident radiation. Since V_{out} is from 5 to 10 times greater than V_{in}, it was possible to cause V_{out} to be a measurable amount nonlinear before V_{in} was affected. This saturation was then noted as an abrupt change in the apparent transmission and V_{out} was noted as the limiting output voltage.

The above was repeated for various values of the high voltage supplied to the divider circuit and the corresponding limiting voltages were noted.

Neutral pass optical filters could then be used during the tests to assure that the detectors were used in this linear range.

REFERENCES

1. Page, William A., Canning, Thomas N., Craig, Roger A., and Stephenson, Jack D.: Measurements of Thermal Radiation of Air From Stagnation Region of Blunt Bodies Traveling at Velocities Up to 31,000 Feet Per Second. NASA TM X-508, 1961.

2. Page, William A.: Shock-Layer Radiation of Blunt Bodies Traveling at Lunar Return Entry Velocities. IAS Paper 63-41, 1963.

3. Stephenson, Jack D.: Radiation From Wakes of Blunt Bodies at Speeds Up to 32,000 Feet Per Second. NASA paper presented to Antimissile Research Council April 1962, Inst. for Defense Analyses, Wash., D. C.

4. Carnevale, E., and Recesso, J.: Absolute Measurements of Radiation From Ablating Surfaces. Tech. Memo. RAD-9-TM-59-62, AVCO Corp. Research and Advanced Development Div., 1959.

5. Lapple, C. E., Brady, A. P., and Chamberlain, D. L., Jr.: Mechanism of Ablation of Char-Forming Ablative Plastics. ASD Tech. Rep. 61-204, Stanford Research Institute, 1961.

6. Meyerott, R. E., Sokoloff, J., and Nicholls, R. W.: Absorption Coefficients of Air. Geophysical Research Papers No. 68, GRD-TR-60-277, LMSD-288052, July 1960. ASTIA AD-252003.

7. Scala, Sinclaire M., and Gilbert, Leon M.: The Thermal Degradation of a Char Forming Plastic During Hypersonic Flight. American Rocket Society, Space Flight Report to the Nation, New York, Oct. 9-15, 1961.

8. Howe, John Thomas: Shielding of Partially Reflecting Stagnation Surfaces Against Radiation by Transpiration of an Absorbing Gas. NASA TR R-95, 1961.

9. Roberts, Leonard: Mass Transfer Cooling Near the Stagnation Point. NACA TN 4391, 1958.

10. Kemp, Nelson H., Rose, Peter H., and Detra, Ralph W.: Laminar Heat Transfer Around Blunt Bodies in Dissociated Air. Jour. Aero/Space Sci., vol. 26, no. 7, July 1959, pp. 421-30.

11. Boison, J. Christopher, and Curtiss, Howard A.: An Experimental Investigation of Blunt Body Stagnation Point Velocity Gradient. American Rocket Soc. Jour., vol. 29, no. 2, Feb. 1959, pp. 130-5.

12. Chamberlain, D. L., Jr., Van Sickle, D. E., and Marynowski, C. W.: A Study of the Mechanism of Ablation of Reinforced Plastics. WADC Tech. Rep. 59-668, pt. II, 1961.

13. Hilsenrath, Joseph, and Beckett, Charles W.: Tables of Thermodynamic Properties of Argon-Free Air to 15,000° K. N. B. S., AEDC TN 56-12, Sept. 1956.

14. Savin, Raymond D., Gloria, Hermilo R., and Dahms, Richard G.: The Determination of Ablative Properties of Materials in Free-Flight Ranges. NASA TN D-1330, 1962.

15. Vojvodich, Nick S.: The Performance of Ablative Materials in a High Energy, Partially Dissociated, Frozen Nitrogen Stream. NASA TN D-1205, 1962.

16. Tourin, Richard H.: Monochromatic Radiation Pyrometry of Hot Gases, Plasmas, and Detonations. Temperature, Its Measurement and Control in Science and Industry. Vol. III, pt. 2, sec. 43, A. I. Dahl, ed., Reinhold, N. Y., 1962, pp. 455-466.

17. Angstrom, A. K., and Drummond, A. J.: Fundamental Principles and Methods of Calibration of Radiometers for Photometric Use. Applied Optics, vol. 1, no. 4, July 1962.

TABLE I.- SUMMARY OF TEST PARAMETERS AND RESULTS

Material	V_∞, km/sec	ρ_∞/ρ_o	$\dot{q}_a$, watts/cm^2	$\dot{m}$, gm/cm^{2}sec	T_e, ^oK	T_w, ^oK	$\dot{q}_c$, watts/cm^2
Aluminum	6.47	0.02025	---	---	---	---	---
	6.22	.0800	---	---	---	---	---
	5.93	.1974	---	---	---	---	---
Lexan	6.56	.02025	21.5	0.887	7,450	1,000	11,600
	6.82	.02025	36	.9435	7,660	1,000	13,200
	5.90	.02025	14.5 - 17.5	.78	6,950	1,000	8,400
	7.62	.02025	32.4	1.08	8,290	1,000	18,100
	6.08	.0800	69	1.587	7,570	1,000	18,400
	5.75	.0800	37	1.463	7,228	1,000	15,400
	4.54	.1974	25.2	1.556	5,700	1,000	12,000
	5.88	.1974	83	2.386	7,710	1,000	26,200
	6.72	.1974	190	2.873	8,594	1,000	39,000
G.E. 124	6.83	.02025	5.64	.934	7,665	1,550	13,000
	6.125	.0800	17.0	1.60	7,560	1,890	14,700
	6.275	.1974	29 - 32.6	2.61	8,120	2,220	31,800
Polyethylene	6.89	.02025	2.1	.816	7,710	1,000	13,500
	6.08	.0800	8.3	1.326	7,560	1,000	18,400
	5.88	.1974	21.2	1.961	7,680	1,000	26,000

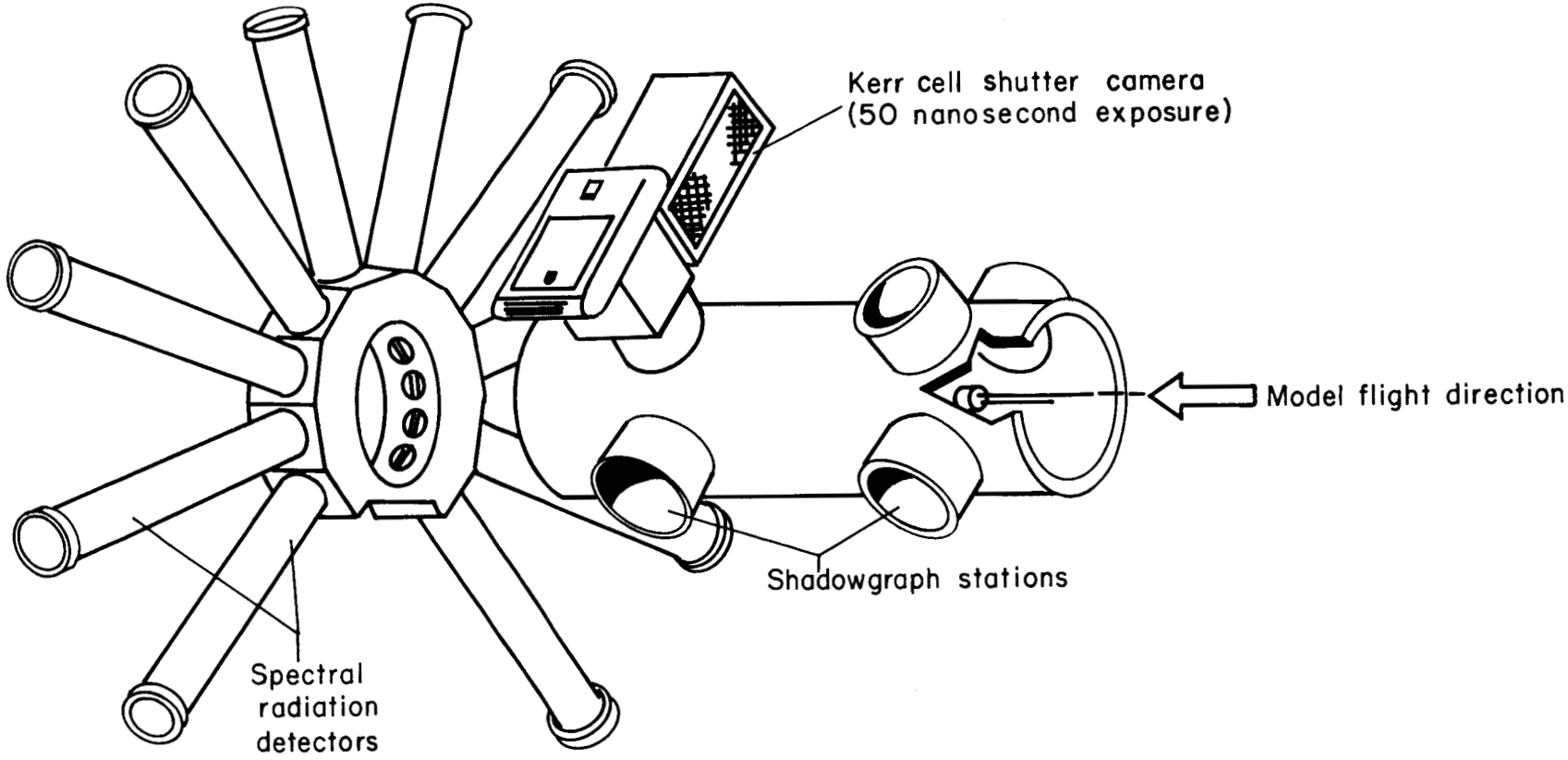

Figure 1.- Schematic representation of test section.

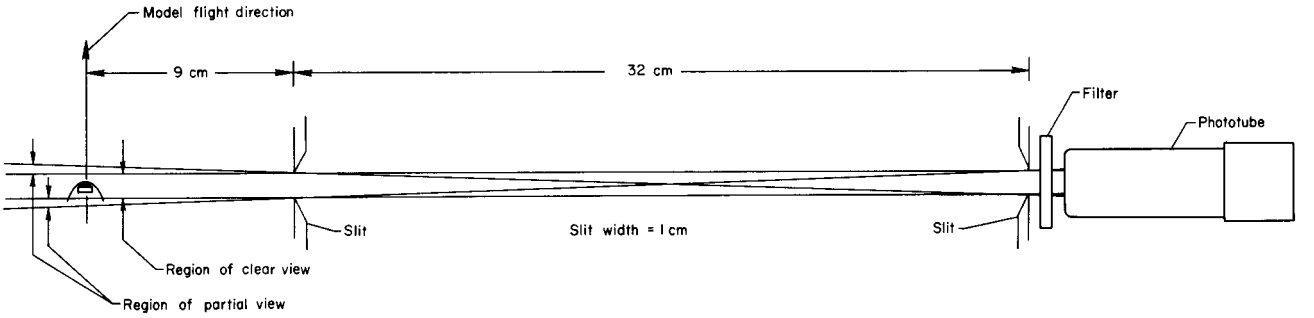

Figure 2.- Schematic drawing of spectral detector showing slit assembly and light path.

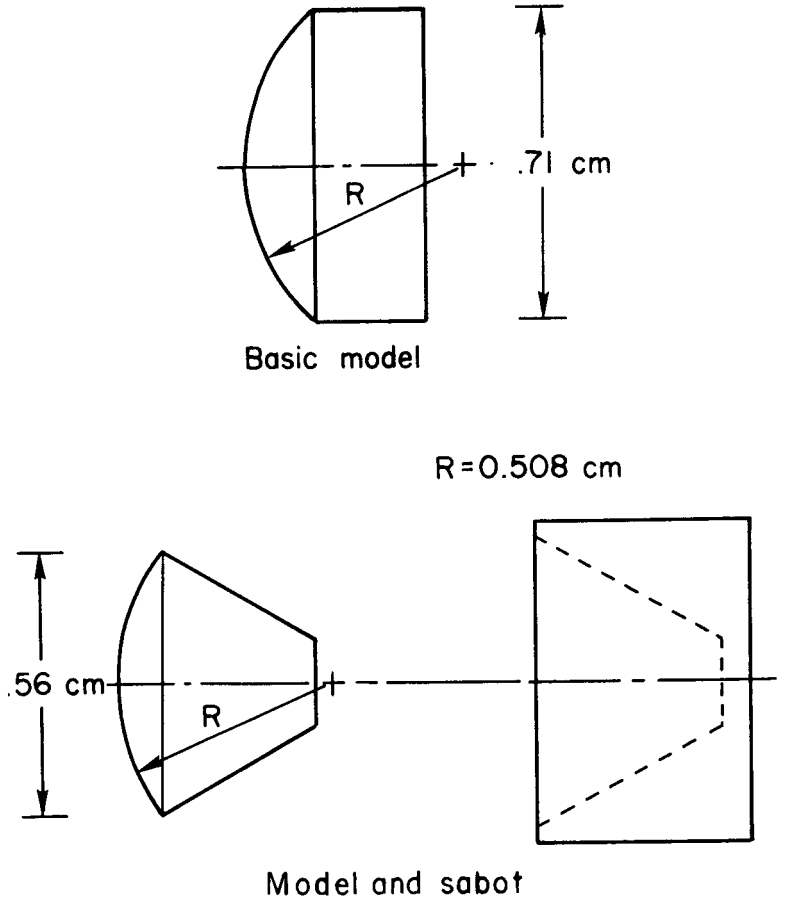

Figure 3.- Test models.

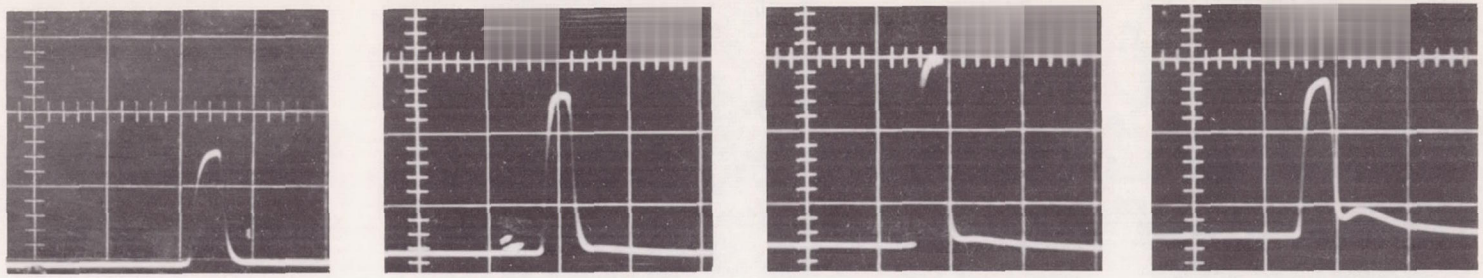

λ_o = 0.235μ λ_o = 0.265μ λ_o = 0.312μ λ_o = 0.369μ

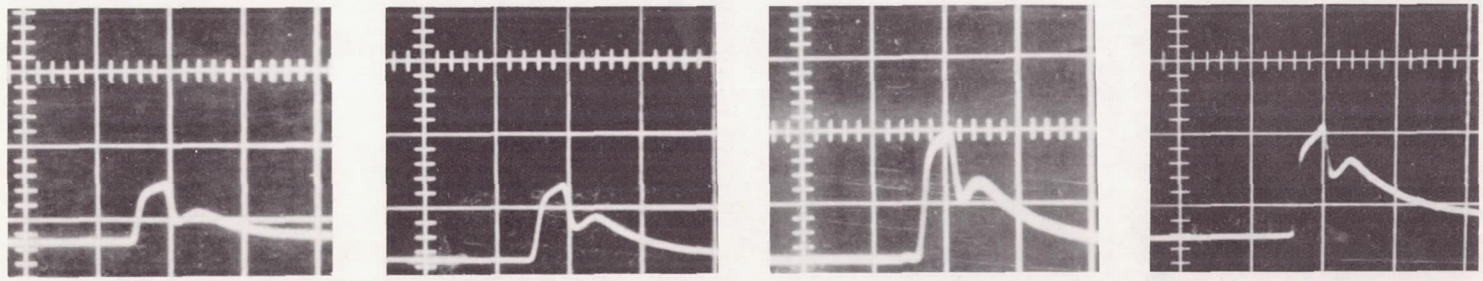

λ_o = 0.460μ λ_o = 0.518μ λ_o = 0.661μ λ_o = 0.942μ

Figure 4.- Set of phototube signals recorded during a typical test. Sweep rate is 5 microseconds per large division.

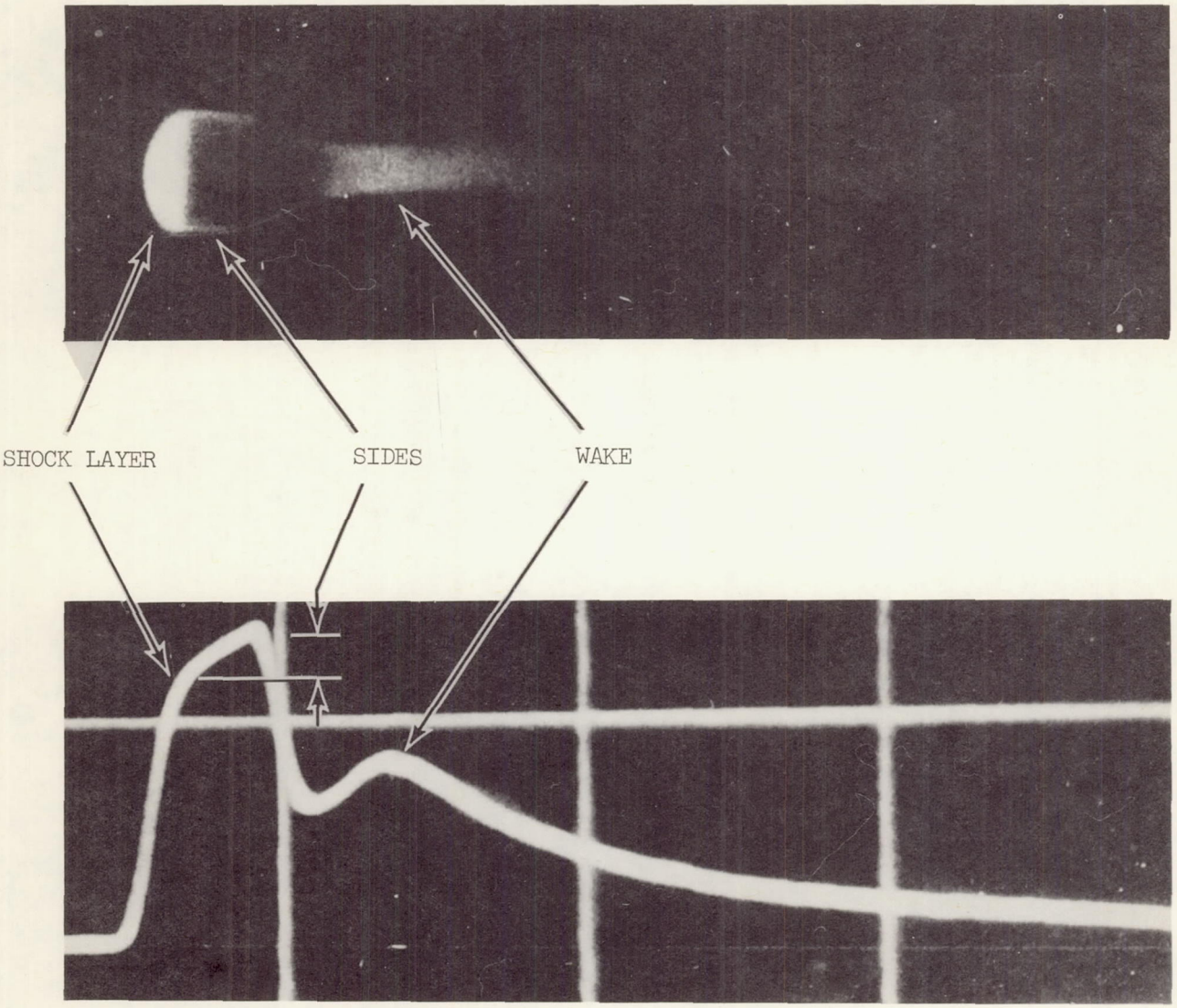

Figure 5.- Self-luminous photograph and oscilloscope record showing relationship between luminosity about model and phototube signal.

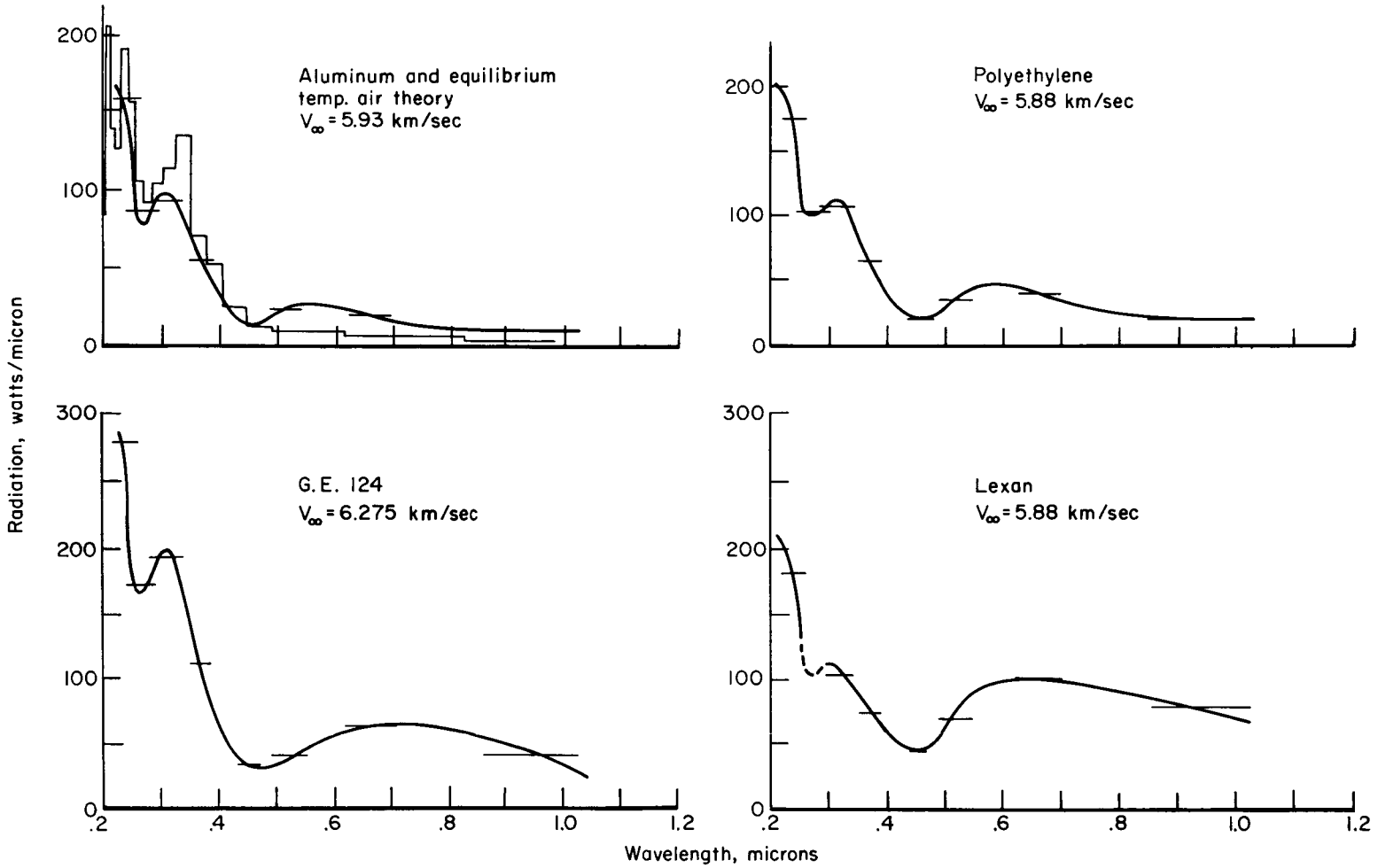

(a) $\rho_\infty/\rho_o = 0.2$

Figure 6.- Shock-layer-region spectrographic data obtained from models.

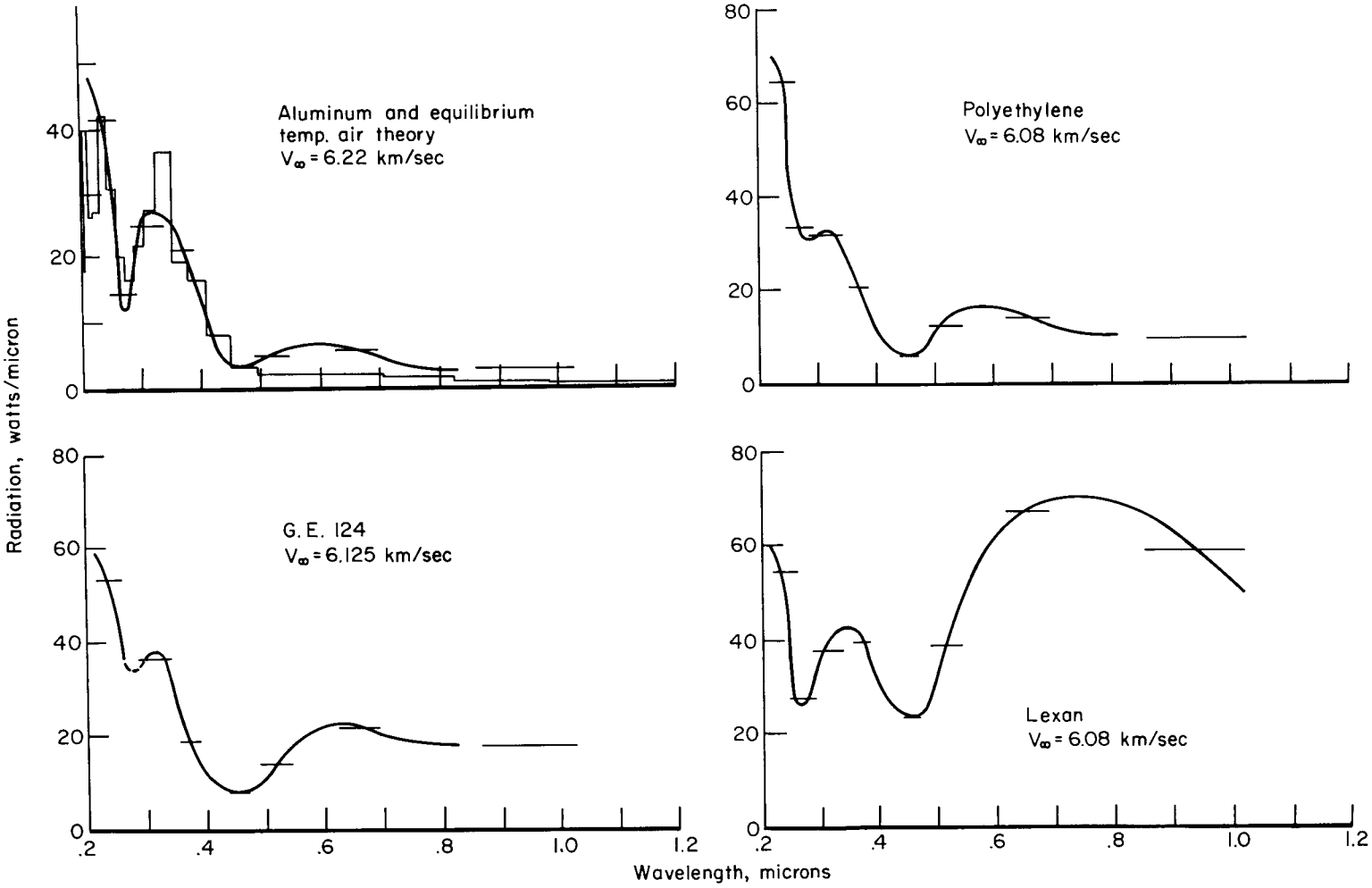

(b) $\rho_\infty/\rho_o = 0.08$

Figure 6.- Continued.

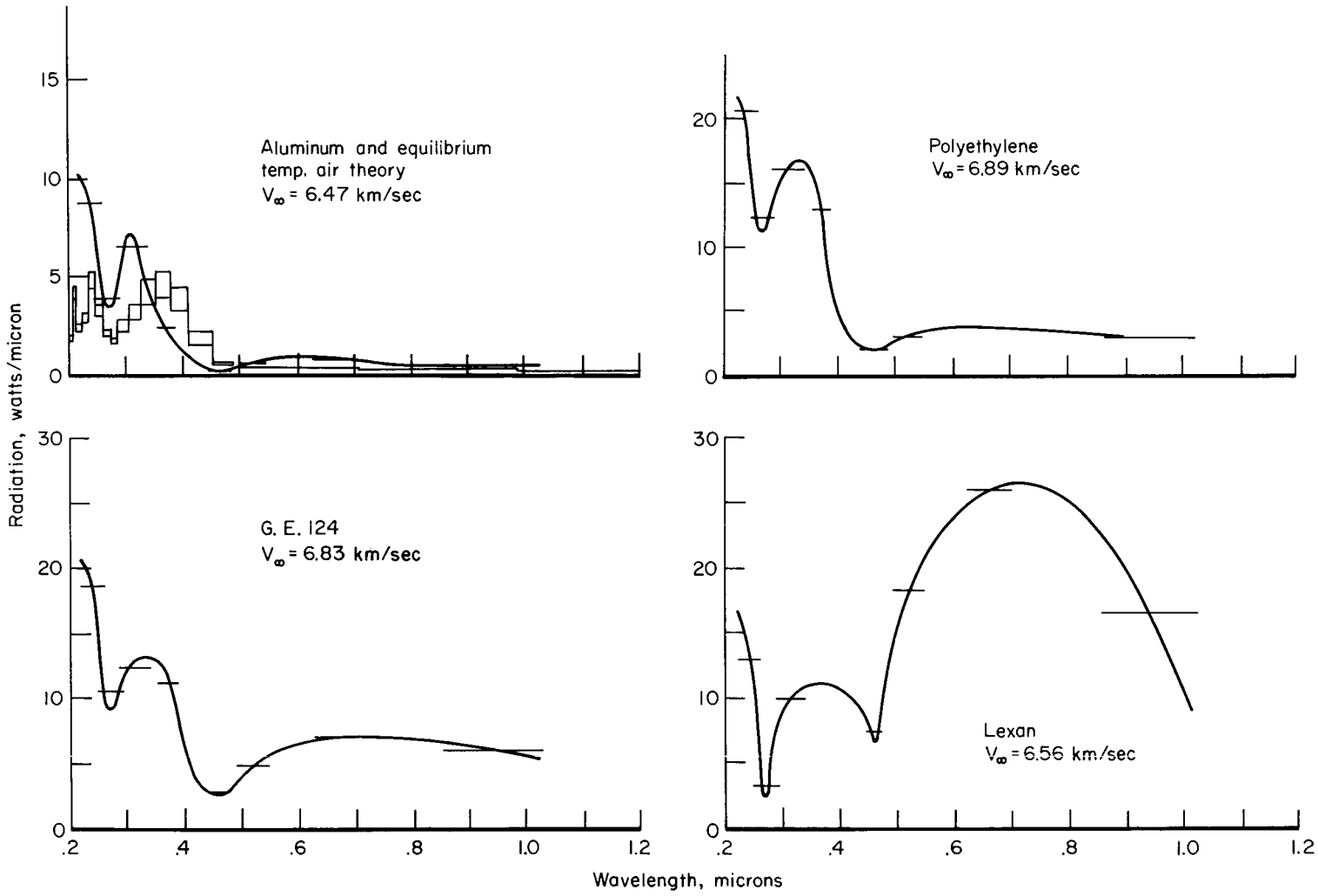

(c) $\rho_\infty/\rho_o = 0.02$

Figure 6.- Concluded.

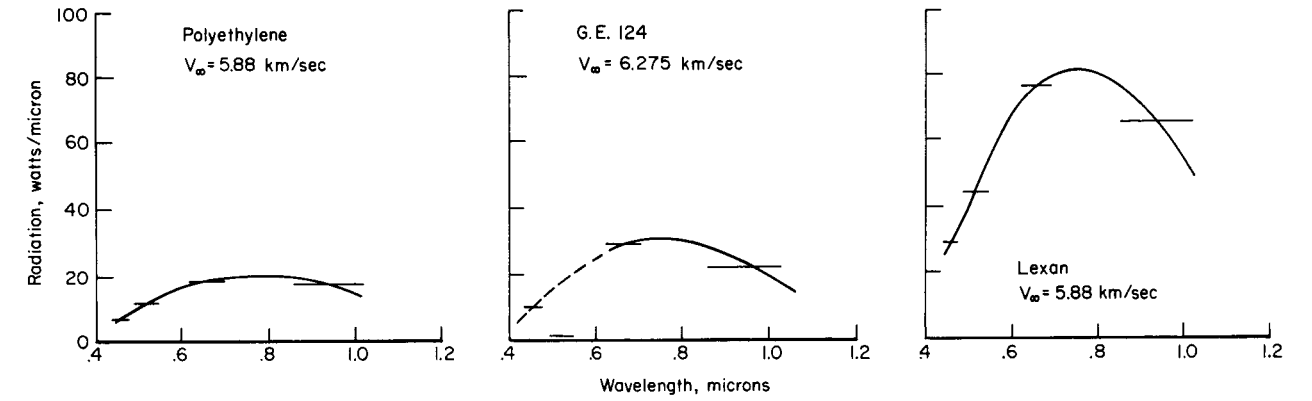

(a) $\rho_\infty/\rho_o = 0.20$

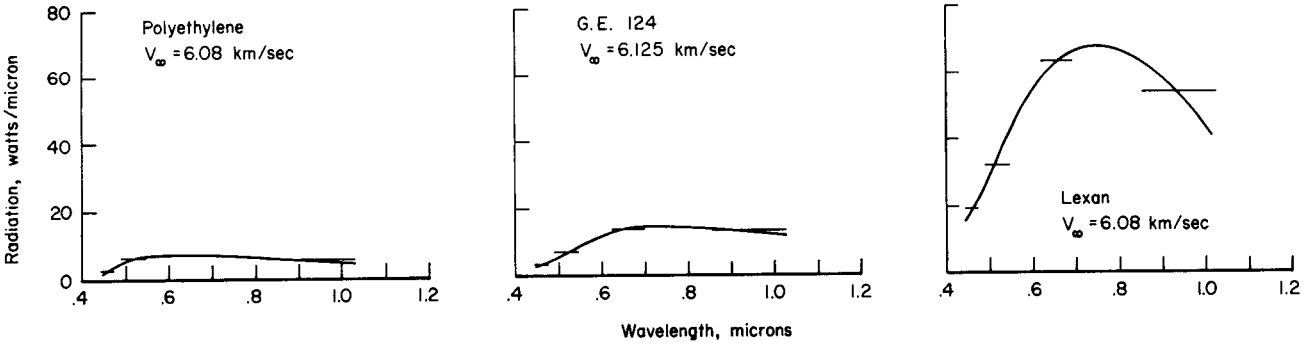

(b) $\rho_\infty/\rho_o = 0.08$

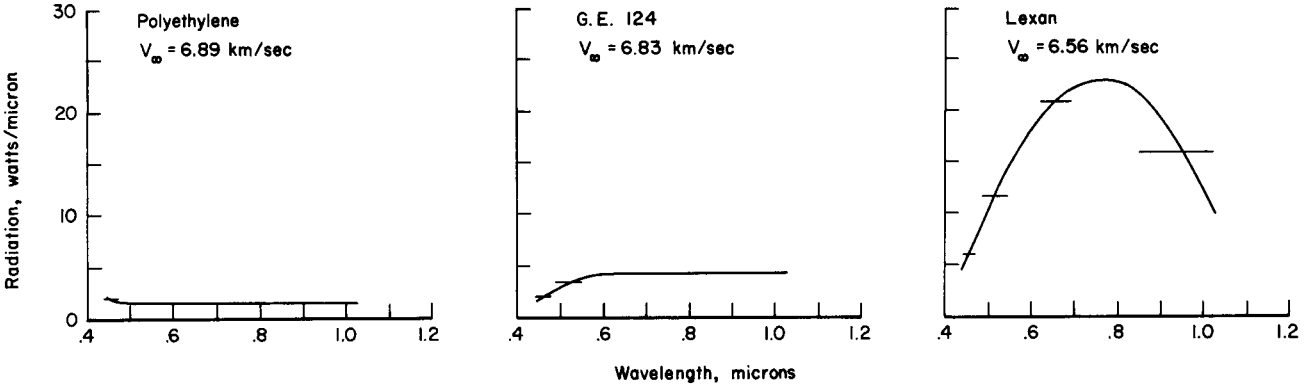

(c) $\rho_\infty/\rho_o = 0.02$

Figure 7.- Spectra of ablation product radiation from the shock layer of models.

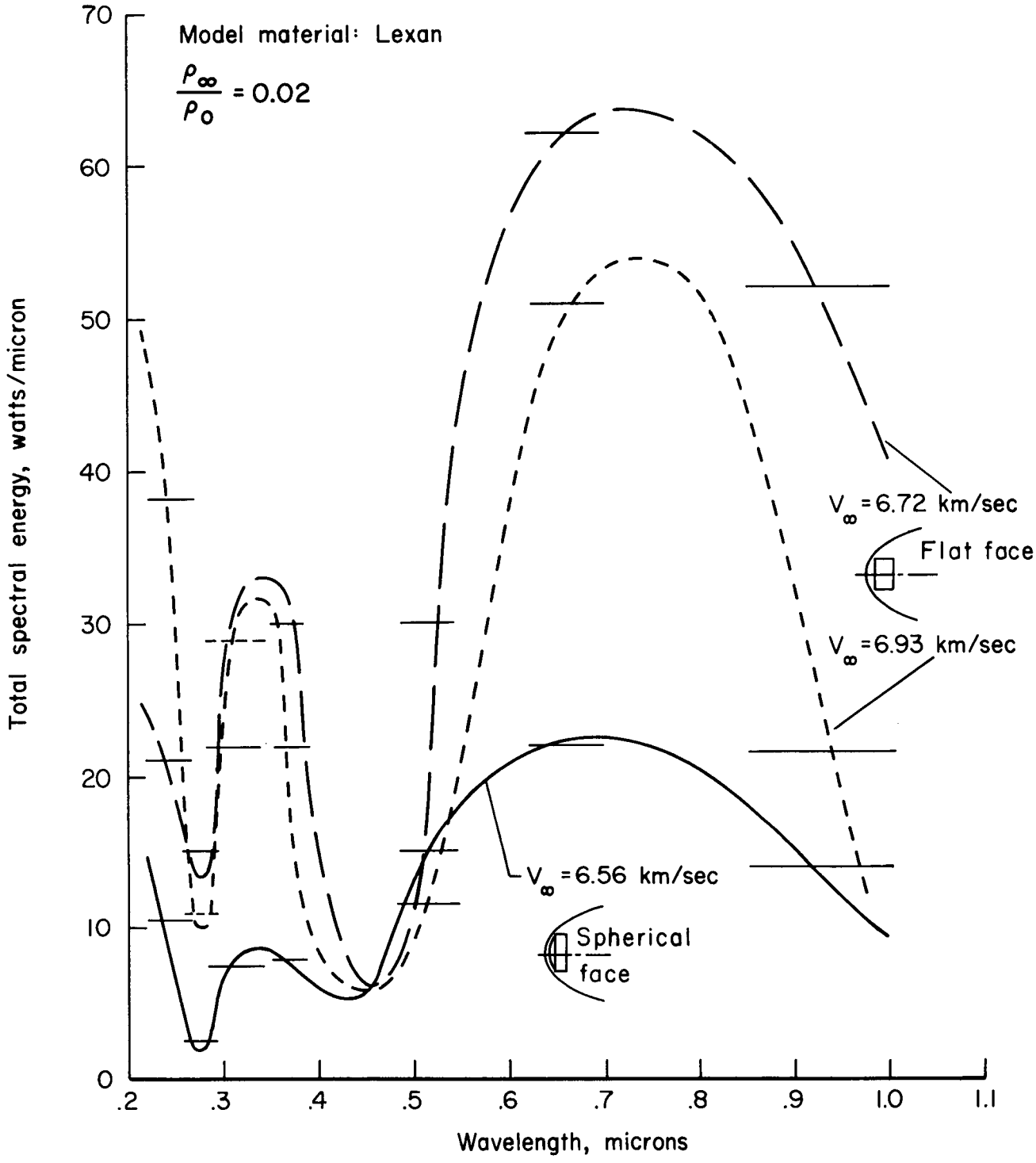

Figure 8.- Comparison of spectra from right circular cylindrical and basic model configurations.

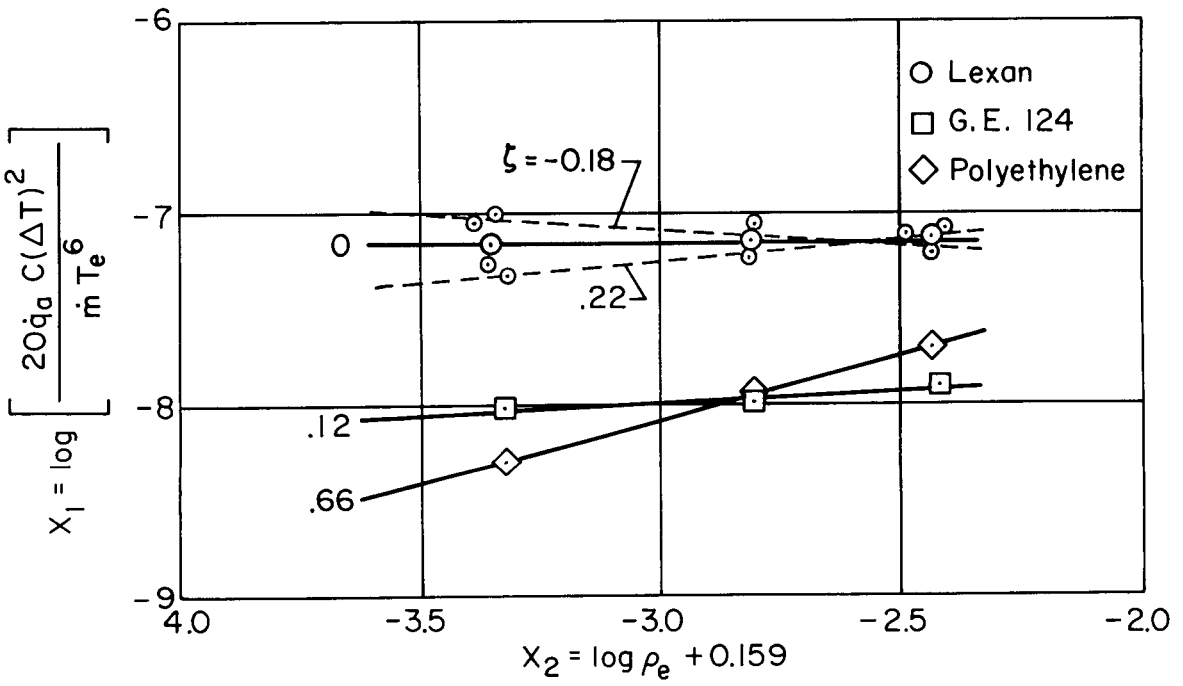

Figure 9.- Determination of ζ from test data.

NASA-Langley, 1963 A-685